Magnetic field measurements

- azimuth of the magnetic field from linear polarization(ambiguity in orientation):
  $\phi = 0.5 \arctan(U/Q)$
- strength of L.O.S magnetic field from zeeman shift

First vector magnetic field inferences along an individual, resolved coronal loop structure extending up to heights of 70 Mm (0.1 RSun) and the first polarimetric measurements of coronal loops located **on disk**
Off-limb studies in optically thin spectral lines must take into account LOS integration effects

Other off limb magnetic field measurements

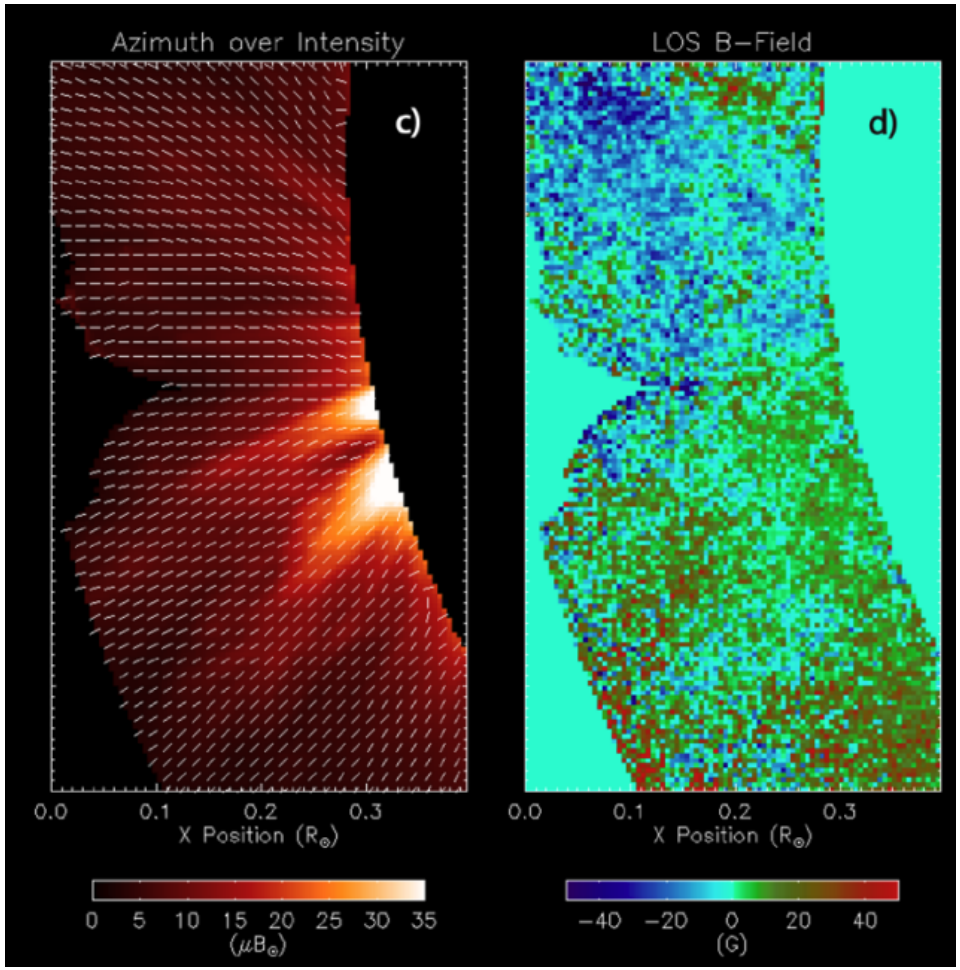

Figure 1: Tomczyk et al. 2008 measurements: left intensity with superimposed vectors showing the plane of sky direction of the magnetic field, right: the LOS component of the magnetic field

Other off limb magnetic field measurements

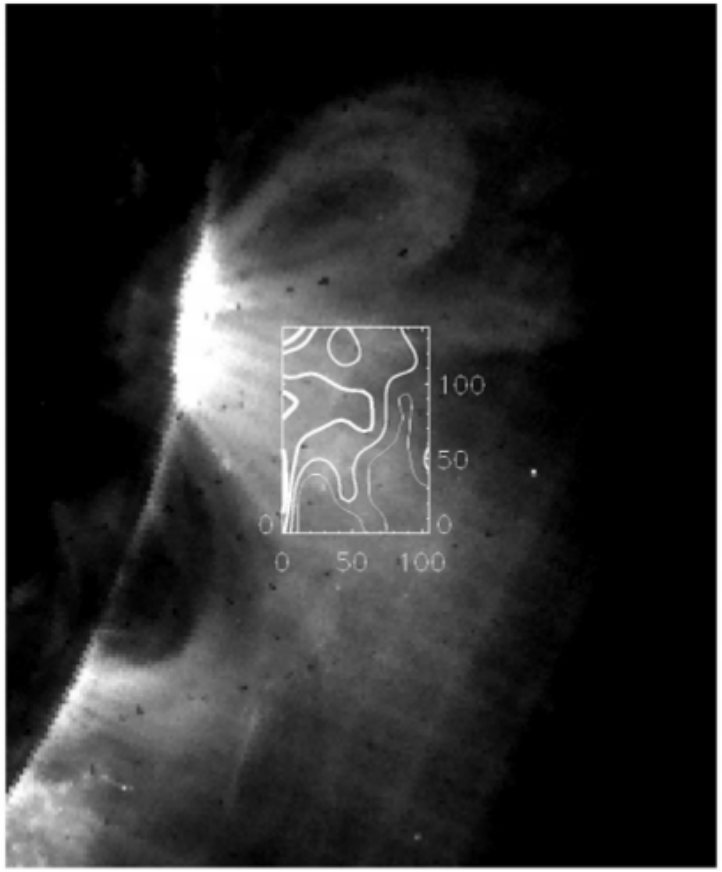

FIG. 3.—Contour map (based on 20″ pixels) of the measured coronal magnetic field strength using Fe XIII overplotted on the EIT Fe XV image. The thick contour corresponds to 4 G, with additional contours corresponding to flux densities of 2, 0, and −2 G. Tick marks indicate the spatial scale in units of arcseconds.

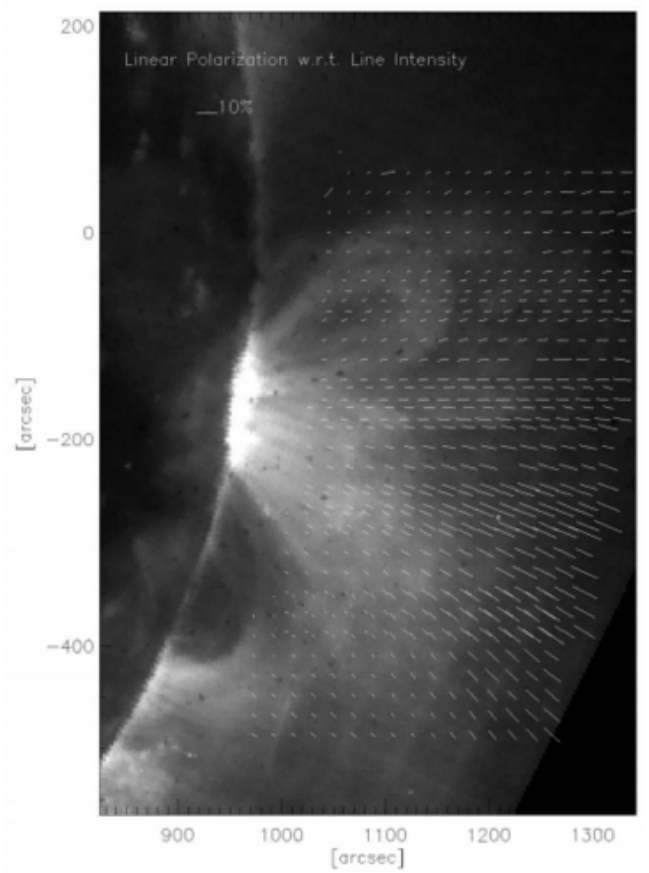

FIG. 2.—Measured linear polarization of Fe XIII for all of the pointings near NOAA AR 581, superposed on an EIT 28.4 nm Fe XV image. The plotted lines show the magnitude and direction of the linear polarization. The overlapping telescope pointings and fiber positions cause the nonuniform spatial sampling.

Figure 2: Lin et al. 2004 measurements (100 arcsec $\approx$ 72.5 Mm)

Magnetic field measurements from seismology

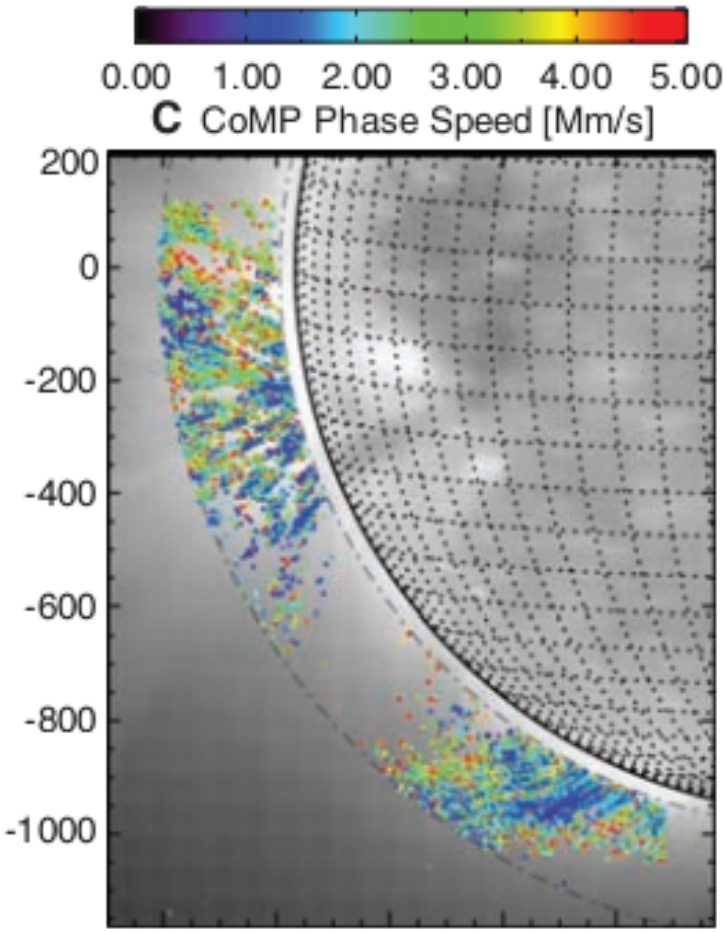

Figure 3: Tomczyk et al. 2007 performed coronal seismology techniques to off-limb observations of the Fe XIII line (at projected heights above 35 Mm) and inferred average coronal magnetic field strengths between 8 and 26 G using the Alfvén wave phase relation:
1) using relationship $v_A = \frac{B}{\sqrt{\mu_0 \rho_c}}$
2)measuring phase speed between 1.2 and 5 Mm/s (Alfvén waves are incompressible, so they are not visible as intensity fluctuations, velocity fluctuations inferred from Doppler shifts of emission)
3)using typical electron density of $10^8/cm^3$

Magnetic field measurements from seismology

Comparison of wave propagation angle with azimuth angle of magnetic field determined from linear polarization measurement (angles relative to solar north-south)

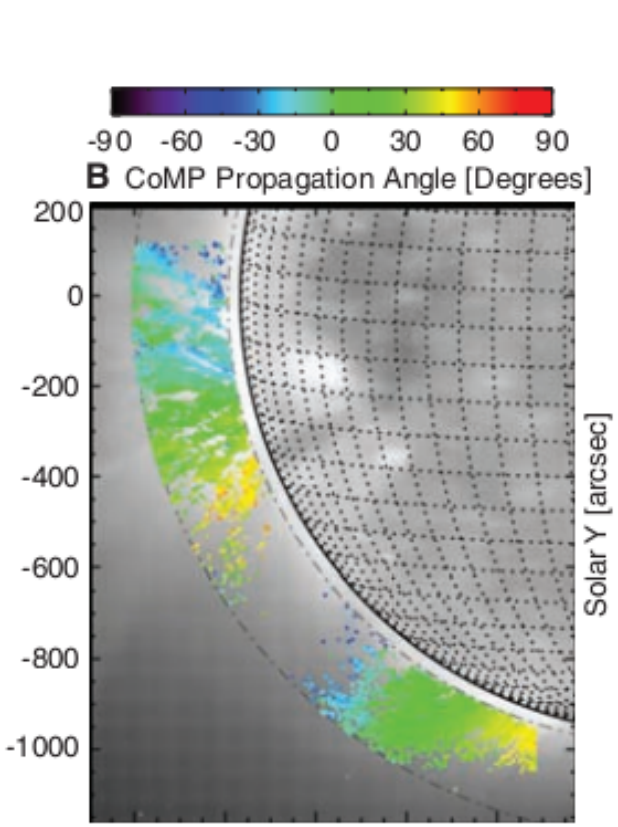

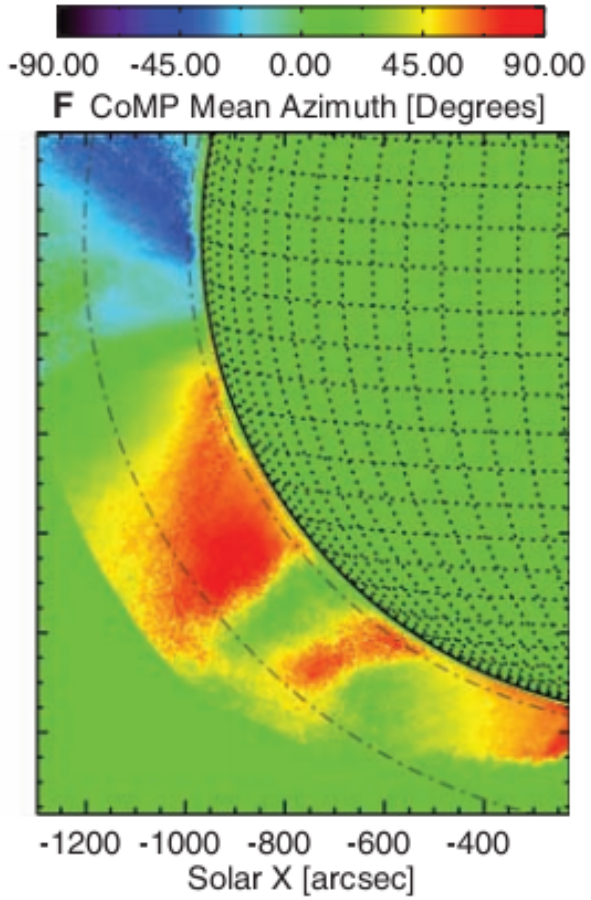

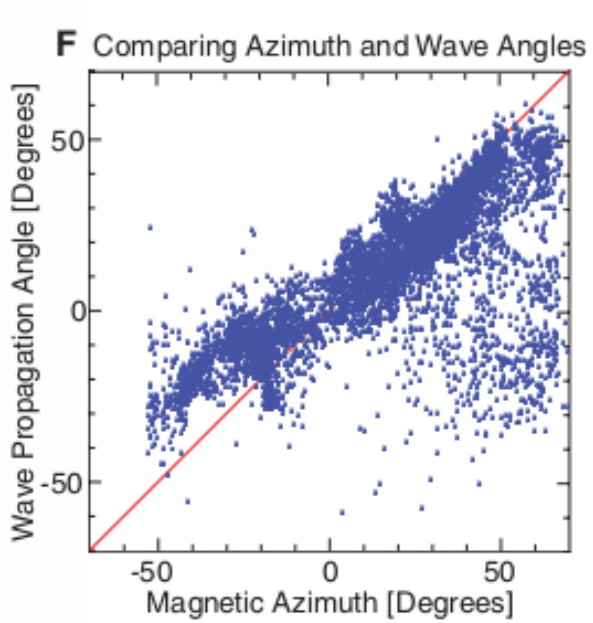

Magnetic field measurements from gyrofrequency

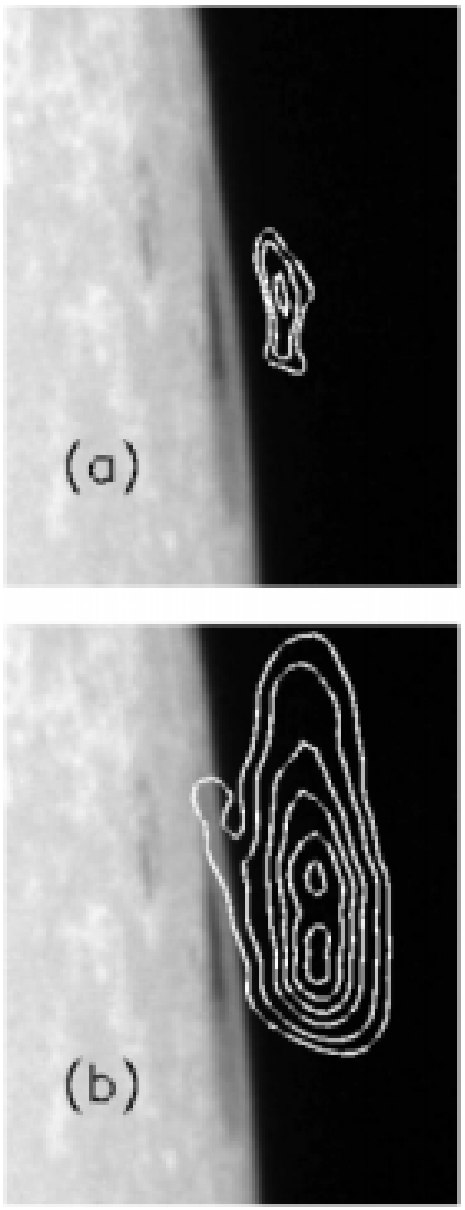

Figure 4: Brosius, White, 2006 determine magnetic field strength by measuring cyclotron frequency of electrons at 15Ghz and 8Ghz (a) 15 GHz radio intensity contours of 1.5, 3.0, and 6.0 $\cdot 10^5$ K; (b) 8 GHz radio intensity contours of 0.125, 0.25, 0.5, 0.75, 1.0 and 1.25 $\cdot 10^6$; K

1) calculate free-free radio brightness temperature at the location of 15Ghz peak: $3.4 \cdot 10^4 K \ll 6.9 \cdot 10^5 K$ observed

2)2 observed peaks for brightness temperature 8Ghz $1.3 \cdot 10^6$, $1.4 \cdot 10^6$ K $\gg 6 \cdot 10^4$K calculated

3) conclude that emission comes mainly from cyclotron

4)use formula $f = \frac{eB}{m_e} \frac{m}{2\pi}$ (m is harmonic number?), conclude that m should be 3 and obtain B = 1750G for the 15Ghz peak location(8Mm) and 960G for the 8Ghz peak location (12Mm above umbral center)

Magnetic field measurements

- cool, neutral material measured in this observation
- upper temperature 15000 - 35000K determined from Doppler widths (in the same HeI line) in accordance with measurements by Ahn and Antolin which found that coronal rain is a multithermal phenomenon with a spatially thin transition between chromospheric and TR temperatures. Meanwhile, their observations suggest a relatively wider, yet still narrow, transition (0.5arcsec) from TR to coronal temperatures
- lower level of HeI maintained by recombination(electrons captured by HeIII and HeII ions) and rapid deexcitation cascade $\Longrightarrow$ the line formation is linked to the availability of ions tied to the magnetic field (similar discussion as in the case of $H\alpha$ line by Antolin and Rouppe van de Voort in order to explain why we expect neutral material to trace the magnetic field)

Partial ionization effects

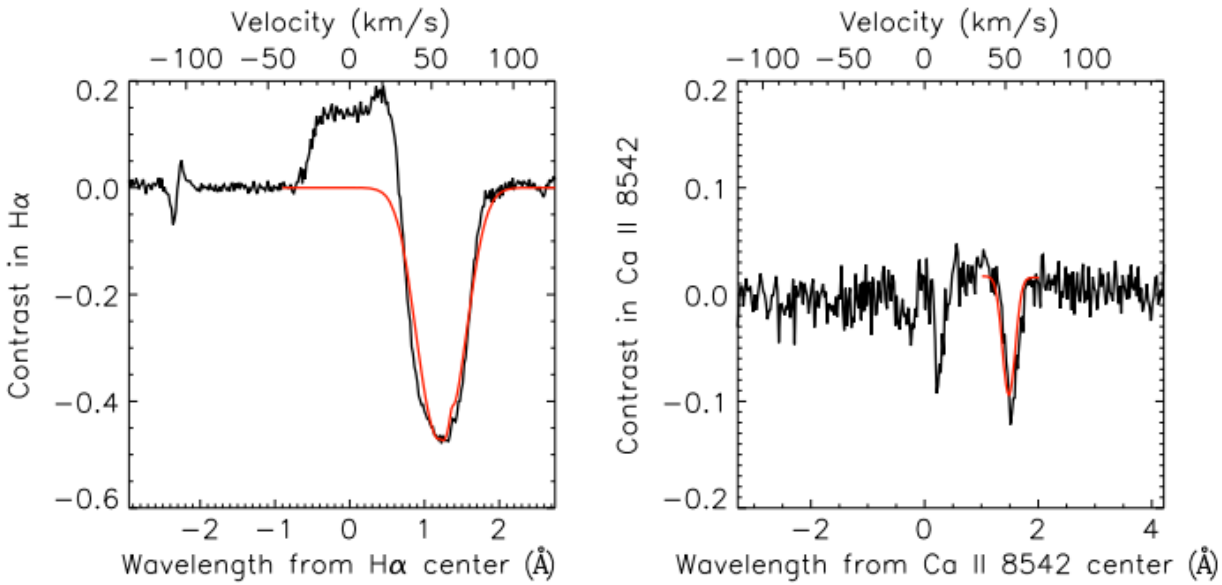

Figure 5: Ahn 2014 measurements showed neutral and ionized species to fall in unison

Partial ionization effects

ions and neutrals decoupled which may lead to cross field diffusion

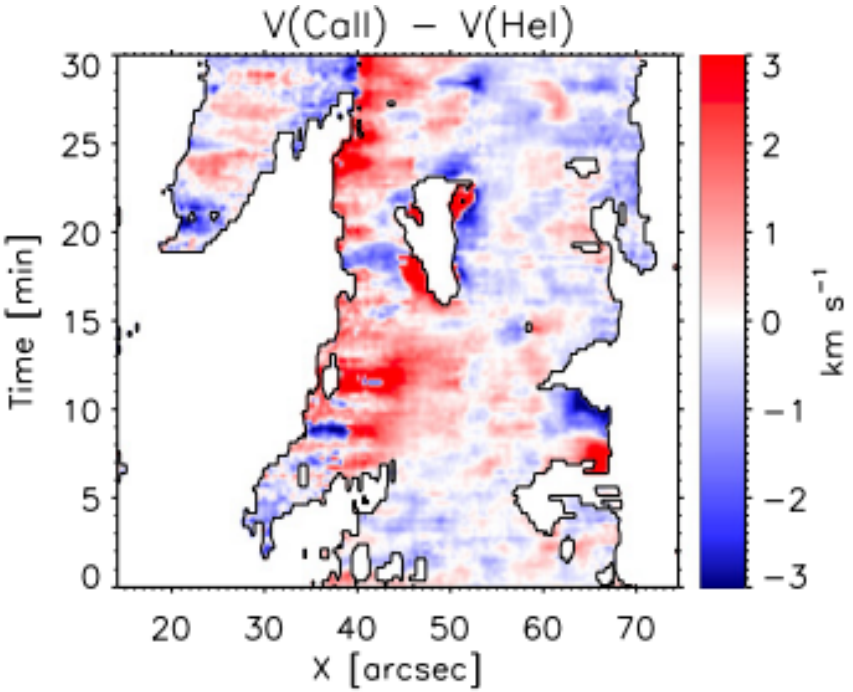

Figure 6: Khomenko et al 2016 measurements showed small differences between neutrals and ions velocities in a solar prominence

Gilbert et al. (2002) calculated the neutral helium cross-field downflow speed to be $8 \cdot 10^3$ cm/s , while values reached 10 km /s for prominence material of very low density ($10^9 cm^-3$), both of which are small fractions of the velocities observed here

Condensation effects

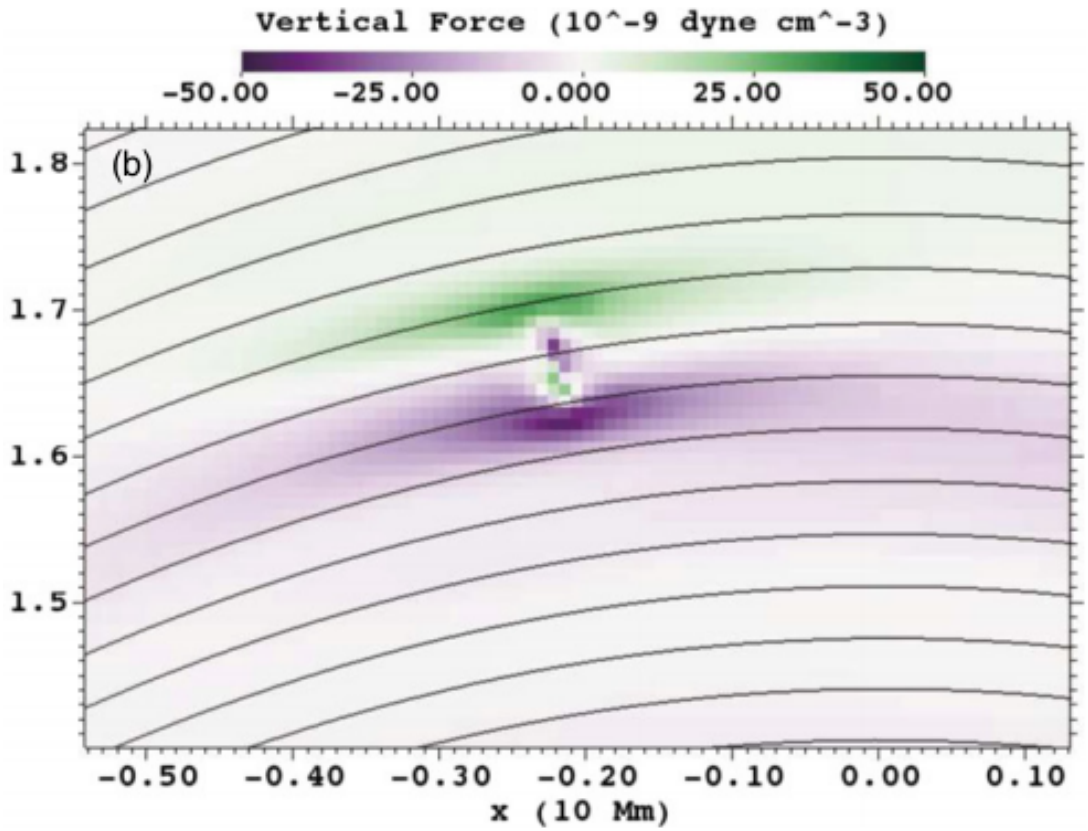

Figure 7: Fang et al. (2013) determined that the pressure gradient brought on by the formation of small, but dense, coronal condensates introduces a force on par with the Lorentz force, and thus the presence of the cool material can induce field variations locally and within its neighborhood

Future improvements

- Daniel K. Inouye Solar Telescope:
  substantial increase of light-gathering capability
- new diagnostics techniques such as the use of the He I polarization as a height diagnostic Asensio Ramos et al. 2008:
  determining consistently the height-dependent atomic level polarization induced by the anisotropic radiation field within the atmosphere model that provides the best fit to the observed Stokes profiles. Since the anisotropy factor is very sensitive to the source function gradient the solution of these types of problems in stratified model atmospheres may be facilitated by the application of efficient iterative schemes